Multifluid squirt flow and hysteresis effects on the bulk modulus - water saturation relationship

submitted to *Geophys. J. Int.*

Multi-Fluid Squirt Flow and Hysteresis Effects on the Bulk Modulus-Water Saturation Relationship

G. Papageorgiou[1] and M. Chapman[2]

School of Geosciences, Grant Institute, West Mains Road, Edinburgh EH9 3JW, UK.

[1]giorgos.papageorgiou@ed.ac.uk

[2]mark.chapman@ed.ac.uk

SUMMARY

Many applications of seismology require the calculation of wavespeed and attenuation in rocks saturated with multiple fluids. Squirt-flow is known to be an important effect in fully saturated rocks but the extension to the multi-fluid case is unclear. Neglecting capillary effects, we generalise previous work on squirt-flow to the case where two fluids are present. We derive expressions for the effective fluid properties, but the results depend on the spatial distributions, and not only volume fractions, of the two fluids. Our results demonstrate that such multi-fluid squirt-flow may be responsible for hysteresis effects in elastic properties during imbibition and drainage.

1 INTRODUCTION

Determining the quantitative relationship between fluid saturation and seismic characteristics such as wave velocity and attenuation, is a challenging problem in geophysics. It has various applications ranging from accurate determination of gas/oil saturation in seismic surveys, to estimating mobility of CO_2 in carbon capture and storage or enhanced recovery projects. The challenge lies in that it is not entirely understood how the spatial distribution of fluids affects elastic wave propagation.

In a popular approach to the problem of partial fluid saturation, it is assumed that the fluid

forms pockets or patches. Current work by Pham et al. (2002) and more recently Qi et al. (2014a), Qi et al. (2014b) addresses such issues. At the same time, experimental data for partially saturated, anisotropic synthetic rocks show that the diffusion mechanism attributed to squirt-flow is significant as pointed out by Amalokwu et al. (2014).

Wave-induced fluid flow or squirt flow as introduced in Dvorkin et al. (1995) predicts significant dispersion in seismic waves but these theories are confined to full saturation. It is largely accepted that it is a phenomenon due to pressure gradients between elements of the pore space of different compliances and is triggered by passing seismic waves.

In one modelling approach of the squirt flow effect introduced by Chapman et al. (2002), a pore network of compliant microcracks and stiffer pores is used to model the porous medium. The diffusion mechanism at full saturation is then described by a Darcy fluid flow between neighbouring members of this network (selected at random to be microcracks or pores). Within this theory, it is not clear how to approach variable saturations.

In this paper, we present an extension of the micro-structural approach to accomodate the case of partially saturated pores. Rather than assume discrete patches our assumption is that the two immiscible fluids exist within each crack and pore. We also assume that pressure equalisation occurs within each inclusion and we show the result depends on an effective viscosity tied to the relative permeability of each fluid.

Our results demonstrate that the elastic properties depend not only on the volume fraction of each fluid but also on how the fluids are distributed between cracks and pores. We introduce simple conceptual models for imbibition and drainage and find that our model predicts significant hysteresis in the bulk modulus–saturation relationship.

2 THEORY

It was shown in Chapman et al. (2002) that a pore network model can be constructed where fluid exchange between inclusions of different compliance gives rise to a squirt-flow mechanism. Average masses of the saturating fluid represented as $m^{\ominus}, m^{\odot}$, denote the fluid content of two pore types in the pore network: ellipsoidal microcracks and spherical micropores. We index symbols referring to each inclusion, respectively by $^{\ominus}$ and $^{\odot}$. Local flow is then described as a Darcy flow between different types of pores:

$$\partial_t m^{\ominus} = \frac{\rho_0 k \zeta}{\eta}(P^{\odot} - P^{\ominus}) = -\partial_t m^{\odot} \tag{1}$$

where $\tau^{-1} = \frac{\rho_0 k \zeta}{\eta}$ is the diffusivity constant depending on the fluid density ρ_0, matrix permeability k, grain size ζ and fluid viscosity η.

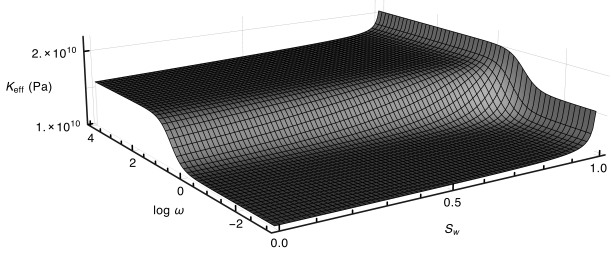

Figure 1. Effective bulk modulus as a function of angular frequency and fluid saturation for our baseline model.

Mass exchange between neighbouring cracks and pores is therefore understood to be driven by their pore pressure difference where each pressure is indicated as $P^{\odot}, P^{\ominus}$ according to our notation. With a suitable description $m(P)$ relating the mass content to the pressure in each inclusion, the above can be solved in the frequency domain and a frequency dependent expression for each pressure can be calculated. These expressions can be used in conjunction with the inclusion theory of Eshelby (1957) to provide an effective elastic tensor. This framework is studied and understood also for cases where inclusions have different relative sizes and a preferred orientation in Chapman (2003). The most general single fluid case was studied by Jakobsen & Chapman (2009)

In the general multi-fluid case, we would have to consider spatial variations in each fluid pressure within each crack and pore. To simplify the problem, we neglect capillary pressure effects and assume a constant fluid pressure in each fluid within each inclusion. This allows us to model grain-scale pressure gradients between inclusions while assuming pressure equilibration with each inclusion.

$$\begin{aligned} \partial_t m_1^{\ominus} &= \frac{\rho_{1(0)} k_1 \zeta}{\eta_1} \left(P^{\odot} - P^{\ominus}\right) = -\partial_t m_1^{\odot} \\ \partial_t m_2^{\ominus} &= \frac{\rho_{2(0)} k_2 \zeta}{\eta_2} \left(P^{\odot} - P^{\ominus}\right) = -\partial_t m_2^{\odot}. \end{aligned} \tag{2}$$

The expressions relating the density of each fluid to its pressure come straight from the definition of the fluid bulk modulus i.e.:

$$\rho \simeq \rho_0 \left(1 + \frac{P_f}{K}\right) \tag{3}$$

and can be applied to each fluid and inclusion pressure. The above would have to be combined with an expression for the volume of each inclusion in terms of stress balance between fluid

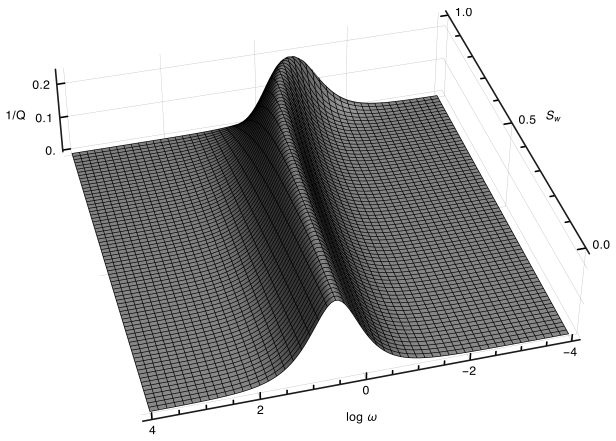

Figure 2. Attenuation of the baseline model as a function of frequency and fluid saturation.

and external stress σ_{ij} :

$$\begin{aligned}\phi^{\ominus} =&\phi_0^{\ominus}\left(1-\frac{\sigma_n}{\sigma_c}+\frac{P^{\ominus}}{\sigma_c}\right)\\ \phi^{\odot} =&\phi_0^{\odot}\left(1-\frac{3}{4\mu}\frac{(1-\nu)}{(1+\nu)}\sigma_{ll}+\frac{3}{4\mu}P^{\odot}\right).\end{aligned} \tag{4}$$

Here, the modulus σ_c depends on the aspect ratio r of the ellipsoid inclusions:

$$\sigma_c = \frac{\pi\mu r}{2(1-\nu)} \tag{5}$$

and, for a sufficiently large collection of inclusions in the representative volume, we can assume the normal stress σ_n is a third of σ_{ll}. The parameter μ denotes the shear modulus of the grains and ν their Poisson's ratio.

The above information suffices to solve (2) assuming a harmonic excitation $\sigma_n(t) = \frac{1}{3}\sigma_{ll}(t) = \sigma\ e^{\mathrm{i}\omega t}$. However, we also need to assume that the fluids are at constant – or at least constant within the modelled time and length scale – relative volume fractions $S_1 = 1 - S_2$. Now we can explicitly calclate the mass content of each fluid which is

$$\begin{aligned} m_1^{\ominus} =&S_1\rho_1^{\ominus}\phi^{\ominus} \quad m_1^{\odot} =S_1\rho_1^{\odot}\phi^{\odot}\\ m_2^{\ominus} =&S_2\rho_2^{\ominus}\phi^{\ominus} \quad m_2^{\odot} =S_2\rho_2^{\odot}\phi^{\odot}.\end{aligned} \tag{6}$$

and it can be seen from (2) that this is equivalent to a single effective fluid theory with parameters

$$\begin{aligned}\widetilde{m}^{\ominus} =&m_1^{\ominus}+m_2^{\ominus} \quad \widetilde{m}^{\odot} =m_1^{\odot}+m_2^{\odot}\\ \frac{1}{\widetilde{K}} =&\frac{S_1}{K_1}+\frac{S_2}{K_2} \qquad \frac{\widetilde{k}}{\widetilde{\eta}} =\frac{k_1}{\eta_1}+\frac{k_2}{\eta_2}.\end{aligned} \tag{7}$$

So in this case, the static component of the theory has an effective fluid modulus given by the Gassmann-Wood average of Domenico (1974). The diffusivity constant still requires the

Table 1. Parameters used in the baseline model.

total porosity:	$\phi_0 = .30$	
crack density:	$\epsilon = 0.05$	
aspect ratio:	$r = 10^{-4}$	
permeability:	$k = 4 \times 10^{-14}$ m^2	
grain size:	$\zeta = 12 \times 10^{-5}$ m	
gas properties:	$\eta_1 = 2 \times 10^{-5}$ Pa s	$K_1 = 2.5 \times 10^7$ Pa
water properties:	$\eta_2 = 10^{-3}$ Pa s	$K_2 = 2.25 \times 10^9$ Pa

definition of a relative permeability model, so for simplicity, we will assume that $k_1 = S_1 k$ and $k_2 = S_2 k$.

With these concessions in mind, we will refer to the above as our baseline model henceforth. This model has a dispersive bulk modulus $K_{\text{eff}}(\omega)$ since each of the fluid pressures calculated in (2) is complex-valued and depends on the harmonic forcing of the external stress field $\sigma(\omega)$ in a linear way. This bulk modulus is calculated as an Eshelby expansion where its zeroth order in ω is the dry modulus K_d and higher order corrections are given as a sum over inclusion types (see Chapman, 2003, eq. 114):

$$K_{\text{eff}}(\omega) = K_d + \phi_0^{\ominus}\left(\frac{K_m}{\sigma_c}+1\right)\frac{P^{\ominus}(\omega)}{\sigma(\omega)} \;+\; \phi_0^{\odot}\left(\frac{3K_m}{4\mu}+1\right)\frac{P^{\odot}(\omega)}{\sigma(\omega)}. \tag{8}$$

The predicted dependence on fluid saturation and frequency can be seen explicitly in Figures 1, 2 depicting respectively its real part and attenuation, calculated as $\frac{\text{Im}(K_{\text{eff}}(\omega))}{\text{Re}(K_{\text{eff}}(\omega))}$. The rock physics parameters for the model are the ones given in Mavko et al. (1998) for a sandstone. The parameters particular to the model are chosen as per Table 1, where the saturating fluids are chosen to match the elasticity of water and gas respectively.

3 MODELLING RESULTS

The above admits a generalisation that is particularly relevant to an inclusion model. Namely, there is no requirement that the partial saturation fractions in the pores and in the microcracks be the same. We will explore this idea further and assume that there are three distinct saturation fractions within the representative volume.

The underlying saturation S_1 is the fluid volume fraction an experimentalist would measure for a sample using information about its porosity and weight. In the case of immiscible fluids, capillary phenomena could be responsible for a different fluid spatial distribution along the narrower microcracks $S_1^{\ominus}$ from that in the pores $S_1^{\odot}$.

The consistency condition these three saturations need to satisfy is that they conserve the underlying fluid volume, thus:

$$\phi_0 S_1 = \phi_0^{\ominus} S_1^{\ominus} + \phi_0^{\odot} S_1^{\odot}, \tag{9}$$

where $\phi_0 = \phi_0^{\ominus} + \phi_0^{\odot}$ and $S_2^{\odot} = 1 - S_1^{\odot},\ S_2^{\ominus} = 1 - S_1^{\ominus}$. Note that in mathematical terms, we are merely changing the implied initial condition for each mass in the differential equations of (2) hence amending the fluid contents in (6).

Now the saturation fractions in (6) become inclusion-dependent which impacts on the effective fluid modulus. By explicitly carrying out the calculation we can show that there is a different effective fluid modulus for each inclusion type that depends on the specific saturation in each inclusion:

$$\begin{aligned} \frac{1}{\widetilde{K}_f^{\ominus}} &= \frac{S_1^{\ominus}}{K_1} + \frac{S_2^{\ominus}}{K_2} \\ \frac{1}{\widetilde{K}_f^{\odot}} &= \frac{S_1^{\odot}}{K_1} + \frac{S_2^{\odot}}{K_2}. \end{aligned} \tag{10}$$

This way the effective fluid moduli become decoupled between pores and cracks and the bulk modulus of equation (8) takes the explicit form:

$$\begin{aligned} K_{\text{eff}}(\omega) = K_d - \\ \phi_0^{\ominus}\left(\frac{K_m}{\sigma_c}+1\right)\ \frac{\alpha B_1\ (\beta A_2+1)\ +\ \beta B_2}{1\ -\ (\alpha A_1+1)\,(\beta A_2+1)} - \\ \phi_0^{\odot}\left(\frac{3K_m}{4\mu}+1\right)\ \frac{\beta B_2\ (\alpha A_1+1)\ +\ \alpha B_1}{1\ -\ (\alpha A_1+1)\,(A_2\beta+1)}, \end{aligned} \tag{11}$$

with the following definitions:

$$\begin{aligned} \alpha(\omega) &= \mathrm{i}\frac{\phi_0^{\ominus}\omega}{\sigma_c\ \zeta}\frac{\widetilde{\eta}}{\widetilde{k}} & \beta(\omega) &= \mathrm{i}\frac{3\phi_0^{\odot}\omega}{4\mu\ \zeta}\frac{\widetilde{\eta}}{\widetilde{k}} \\ A_1 &= 1+\frac{\sigma_c}{\widetilde{K}_f^{\ominus}} & A_2 &= 1+\frac{4\mu}{3\widetilde{K}_f^{\odot}} \\ B_1 &= K_m & B_2 &= 3K_m\frac{1-\nu}{1+\nu} \end{aligned} \tag{12}$$

In a real experiment, the spatial distribution of fluids between cracks and pores will be different during imbibition and drainage. Our model will therefore predict hysteresis effects.

To demonstrate this we need to model the saturations in cracks and pores consistently. We define the crack fraction c_f as introduced in Endres & Knight (1997):

$$c_f = \frac{\phi_0^{\ominus}}{\phi_0^{\ominus}+\phi_0^{\odot}} = \frac{\frac{4}{3}\pi\epsilon r}{\frac{4}{3}\pi\epsilon r+\phi_0^{\odot}}, \tag{13}$$

where in the second equality we have expressed it in terms of the crack density ϵ and aspect ratio r as given in Chapman et al. (2002).

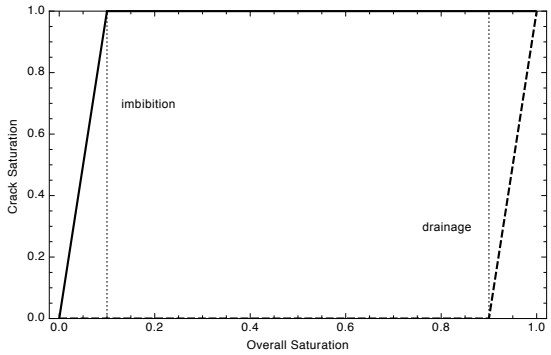

Figure 3. Saturation of cracks versus overall saturation for imbibition (solid) and drainage (dashed). The cracks are saturated and drained before the pores in this example corresponding to a water-wet pore network where saturation is driven by capillary forces.

Now (9), can be re-formulated to the following:

$$S_1 = c_f S_1^{\ominus} + (1 - c_f) S_1^{\odot}. \tag{14}$$

Let us assume that at a critical underlying saturation S_c, there is maximal difference in saturation between cracks and pores $|S_1^{\ominus} - S_1^{\odot}|$. We can write for the respective saturations at $S_1 = S_c$:

$$\begin{aligned} S_1^{\ominus}(S_c) &= \alpha S_c, \\ S_1^{\odot}(S_c) &= \frac{1 - \alpha c_f}{1 - c_f} S_c \end{aligned} \tag{15}$$

for some coefficient α with $0 < \alpha < 1/S_c$. By letting the variation in crack/pore saturation be linear, using (14) the coefficient α determines whether the cracks are imbibed (resp. drained) before or after the pores. Modelling hysteresis amounts to taking a different value of S_c and α in imbibition and drainage.

We will use $S_c^{(imb.)} = 10\%$ and $\alpha = 10$ to denote that during imbibition, the cracks become fully saturated when an underlying saturation of 10% is reached. For drainage, we will use $S_c^{(dr.)} = 90\%$ and $\alpha = 0$ which means the cracks are drained completely when the matrix is drained to an underlying saturation of 90%. Note that S_c is itself constrained to lie between $c_f < S_c < 1 - c_f$.

Using the same lithology and fluids as before, we can now model hysteresis with the above saturation curves for the two processess. The choices of $S_c^{(imb.)}, S_c^{(dr.)}$ can be assumed to have an ideal shape where cracks saturate first under imbibition and drain first during drainage as illustrated in Figure 3. For the values of crack density and aspect ratio in Table 1, the pore saturation is practically indistinguishable from the underlying saturation.

The dispersive mechanism attenuates the seismic waves differently during imbibition and

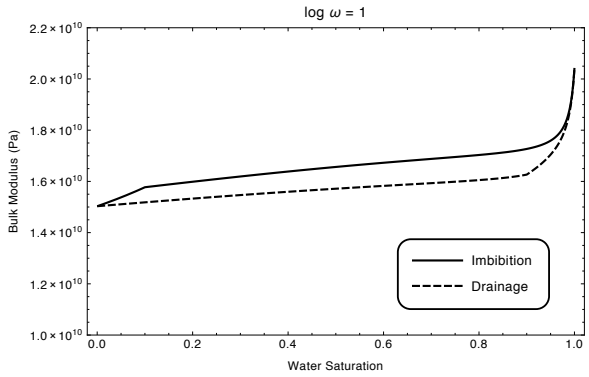

Figure 4. Bulk modulus-water saturation relationship for imbibition and drainage modelled based on the curve of Figure 3.

drainage which is depicted in Figures 4 - 5. By construction, this model matches that of Chapman et al. (2002) for a fully saturated matrix.

4 DISCUSSION

It is widely accepted that the Biot-Gassmann theory underestimates the amount of dispersion exhibited in waves propagating through sedimentary rocks. The likely cause of this excess dispersion is non-uniformity of fluid pressure across the pore space. This may be due to the non-uniformity of the pore space itself (e.g. O'Connell & Budiansky, 1977) or the existence of two saturating fluids (e.g. White, 1975).

The model of Murphy et al. (1986) considers both variations in pore-space geometry and partial gas saturation. His work produces intuitively appealing relationships between attenuation and partial saturation and appears to match experimental data. In a parallel development, Mavko & Jizba (1991) and Dvorkin et al. (1995) show how variations of pore-space geometry give rise to significant dispersion in fully saturated rocks. A consistent description of such effects using inclusion models was given by Chapman et al. (2002) and Jakobsen & Chapman (2009).

Many of the most successful models for partial saturation underestimate dispersion when a single fluid is present. White (1975) contains no dispersion mechanism in the absence of gas while Gurevich et al. (2010) developed an analogue of the model by Murphy et al. (1986) for full saturation which predicts reasonable dispersion.

This paper presents a multi-fluid model which reduces to the local flow model of Chapman et al. (2002) in the full saturation limit. Our results are similar in outline to those in Murphy et al. (1986) and White (1975) but the dependence on the geometry of the saturation is

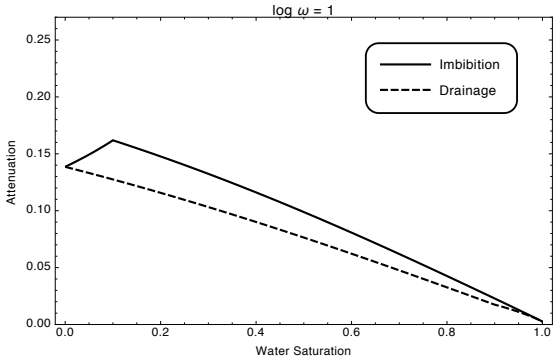

Figure 5. Attenuation-water saturation relationship for imbibition and drainage modelled based on the curve of Figure 3.

different. This dependence on fluid distribution at the pore scale cannot be captured entirely by either the "uniform" or "patchy" saturation concepts.

5 CONCLUSIONS

We have presented a simple extension of the model of Chapman et al. (2002) to the case of multiple fluid saturation. In this study we ignore capillary pressure effects but allow for pore-pressure gradients on the grain scale. Our results indicate that the behaviour is sensitive to the spatial distribution of fluids between cracks and pores so that, e.g., seismic velocity cannot be considered to be a function of water saturation alone.

We calculate the bulk modulus and attenuation as functions of water saturation for idealised models of imbibition and drainage and conclude that multi-fluid squirt flow effects give rise to significant hysteresis effects.

6 ACKNOWLEDGEMENTS

This work was carried out within the DiSECCS project `https://www.bgs.ac.uk/diseccs`. DISECCS is funded by the Engineering and Physical Sciences Research Council (EPSRC) UK. We gratefully acknowledge the constructive reviews of Boris Gurevich and an anonymous reviewer.

REFERENCES

Amalokwu, K., Best, A. I., Sothcott, J., Chapman, M., Minshull, T., & Li, X.-Y., 2014. Water saturation effects on elastic wave attenuation in porous rocks with aligned fractures,

Geophysical Journal International, **197**(2), 943–947.

Chapman, M., 2003. Frequency-dependent anisotropy due to meso-scale fractures in the presence of equant porosity, *Geophysical Prospecting*, **51**(5), 369–379.

Chapman, M., Zatsepin, S. V., & Crampin, S., 2002. Derivation of a microstructural poroelastic model, *Geoph. Jour. Int.*, **151**(2), 427–451.

Domenico, S., 1974. Effect of water saturation on seismic reflectivity of sand reservoirs encased in shale, *Geophysics*, **39**(6), 759–769.

Dvorkin, J., Mavko, G., & Nur, A., 1995. Squirt flow in fully saturated rocks, *Geophysics*, **60**(1), 97–107.

Endres, A. L. & Knight, R. J., 1997. Incorporating pore geometry and fluid pressure communication into modeling the elastic behavior of porous rocks, *Geophysics*, **62**(1), 106–117.

Eshelby, J., D., 1957. The determination of the elastic field of an ellipsoidal inclusion, and related problems, *Proc. R. Soc. Lond. A.*, **241**(1226), 376–396.

Gurevich, B., Makarynska, D., de Paula, O. B., & Pervukhina, M., 2010. A simple model for squirt-flow dispersion and attenuation in fluid-saturated granular rocks, *Geophysics*, **75**(6), N109–N120.

Jakobsen, M. & Chapman, M., 2009. Unified theory of global flow and squirt flow in cracked porous media, *Geophysics*, **74**(2), WA65–WA76.

Mavko, G. & Jizba, D., 1991. Estimating grain-scale fluid effects on velocity dispersion in rocks, *Geophysics*, **56**(12), 1940–1949.

Mavko, G., Mukerji, T., & Dvorkin, J., 1998. The rock physics handbook: Tools for seismic analysis in porous media, 329 pp.

Mayr, S. I. & Burkhardt, H., 2006. Ultrasonic properties of sedimentary rocks: effect of pressure, saturation, frequency and microcracks, *Geophysical Journal International*, **164**(1), 246–258.

Murphy III, W. F., Winkler, K. W., & Kleinberg, R. L., 1986. Acoustic relaxation in sedimentary rocks: Dependence on grain contacts and fluid saturation, *Geophysics*, **51**(3), 757–766.

O'Connell, R. J. & Budiansky, B., 1977. Viscoelastic properties of fluid-saturated cracked solids, *Journal of Geophysical Research*, **82**(36), 5719–5735.

Pham, N. H., Carcione, J. M., Helle, H. B., & Ursin, B., 2002. Wave velocities and attenuation of shaley sandstones as a function of pore pressure and partial saturation, *Geophysical Prospecting*, **50**(6), 615–627.

Qi, Q., Müller, T. M., Gurevich, B., Lopes, S., Lebedev, M., & Caspari, E., 2014a. Quan-

tifying the effect of capillarity on attenuation and dispersion in patchy-saturated rocks, *Geophysics*, **79**(5), WB35–WB50.

Qi, Q., Müller, T. M., & Rubino, J. G., 2014b. Seismic attenuation: effects of interfacial impedance on wave-induced pressure diffusion, *Geophysical Journal International*, **199**(3), 1677–1681.

White, J., 1975. Computed seismic speeds and attenuation in rocks with partial gas saturation, *Geophysics*, **40**(2), 224–232.

Zatsepin, S. V. & Crampin, S., 1997. Modelling the compliance of crustal rocki. response of shear-wave splitting to differential stress, *Geophysical Journal International*, **129**(3), 477–494.